remote sensing

MDPI

Article

High Throughput Field Phenotyping of Wheat Plant Height and Growth Rate in Field Plot Trials Using UAV Based Remote Sensing

Fenner H. Holman [1,*], Andrew B. Riche [2], Adam Michalski [2], March Castle [2], Martin J. Wooster [1,3] and Malcolm J. Hawkesford [2,*]

1 Department of Geography, King's College London, London WC2R 2LS, UK; martin.wooster@kcl.ac.uk
2 Rothamsted Research, Harpenden, Hertfordshire AL5 2JQ, UK; andrew.riche@rothamsted.ac.uk (A.B.R.); adam.michalski@rothamsted.ac.uk (A.M.); march.castle@rothamsted.ac.uk (M.C.)
3 National Centre for Earth Observation (NCEO), Leicester LE1 7RH, UK
* Correspondence: fenner.holman@kcl.ac.uk (F.H.H.); malcolm.hawkesford@rothamsted.ac.uk (M.J.H.)

Academic Editors: Clement Atzberger and Prasad S. Thenkabail
Received: 20 September 2016; Accepted: 14 December 2016; Published: 18 December 2016

Abstract: There is a growing need to increase global crop yields, whilst minimising use of resources such as land, fertilisers and water. Agricultural researchers use ground-based observations to identify, select and develop crops with favourable genotypes and phenotypes; however, the ability to collect rapid, high quality and high volume phenotypic data in open fields is restricting this. This study develops and assesses a method for deriving crop height and growth rate rapidly from multi-temporal, very high spatial resolution (1 cm/pixel), 3D digital surface models of crop field trials produced via Structure from Motion (SfM) photogrammetry using aerial imagery collected through repeated campaigns flying an Unmanned Aerial Vehicle (UAV) with a mounted Red Green Blue (RGB) camera. We compare UAV SfM modelled crop heights to those derived from terrestrial laser scanner (TLS) and to the standard field measurement of crop height conducted using a 2 m rule. The most accurate UAV-derived surface model and the TLS both achieve a Root Mean Squared Error (RMSE) of 0.03 m compared to the existing manual 2 m rule method. The optimised UAV method was then applied to the growing season of a winter wheat field phenotyping experiment containing 25 different varieties grown in 27 m^2 plots and subject to four different nitrogen fertiliser treatments. Accuracy assessments at different stages of crop growth produced consistently low RMSE values (0.07, 0.02 and 0.03 m for May, June and July, respectively), enabling crop growth rate to be derived from differencing of the multi-temporal surface models. We find growth rates range from −13 mm/day to 17 mm/day. Our results clearly display the impact of variable nitrogen fertiliser rates on crop growth. Digital surface models produced provide a novel spatial mapping of crop height variation both at the field scale and also within individual plots. This study proves UAV based SfM has the potential to become a new standard for high-throughput phenotyping of in-field crop heights.

Keywords: Unmanned Aerial Vehicle; Structure from Motion; photogrammetry; crop height; phenotyping

1. Introduction

1.1. Global Food and Agriculture

There is a need to double output of agricultural systems by 2050 to meet the increasing food demands from a growing global population; forecasted to peak at 9.22 billion by 2050 [1,2]. Wheat continues to provide the sole vital daily nutrition for 35% of the world's population [3] and is therefore a key focus of yield improvement research.

Projects such as the 20:20 Wheat® project at Rothamsted Research, aim to provide the knowledge and tools to increase the UK's wheat yield potential to 20 tonnes of wheat per hectare within 20 years [4], whilst combating the new challenges agriculture is facing such as climate change. These projects focus on developing new improved varieties through methods such as selective breeding.

Key to this is the monitoring of different varieties for favourable genotypes and phenotypes, by providing a continuous stream of data documenting the course of the crops development and responses to environmental conditions [5,6].

1.2. Phenotyping

Phenotyping of crops involves the measurement and assessment of physical observable characteristics [7]. Current phenotyping techniques particularly the capacity to collect quality repeatable phenotypic data in field representative growing conditions is a bottleneck for further advancements in knowledge and development of crop varieties and yield gains [8].

Height may be a useful indicator of yield, carbohydrate storage capacity and susceptibility to lodging [9,10] as well as being an essential parameter for site-specific management practices [11]. Monitoring crop height during development stages is a reflection of cultivar and growing conditions. Crop development stages are often defined by the Zadoks Scale [12,13], and in terms of crop growth and height changes the key period of growth in UK grown wheat occurs between the start of stem elongation in early April, stage GS30, and anthesis in mid-June, stage GS61. Anthesis, or flowering, is the point at which crop height is considered to be at maximum [14]. Whilst exact timings of specific development stages will vary between cultivars, it is an important that any method of measuring crop height is able to accurately measure height during all stages between GS30 and GS61 where vegetative structure can vary.

1.3. Measuring Height

Crop height is classified as the shortest distance between the upper boundary of the main photosynthetic tissues on a plant and the ground level [15,16]. Most commonly height data is collected with a measuring rule [10] which although simple, is both laborious, inefficient and can introduce a level of subjectivity into data collected. Applying this method over large trial fields, totalling upwards of 1000 plots, limits the repeatability of this method.

There is a need for rapid, precise, continuous and in-season acquisition of this data [17] in order to better understand external, environmental influences throughout the crops development cycle. Current methods are not sufficient to meet this need, in particular for use in crop trials where the number of measurements required is large and as such development of new technologies and methods is needed.

Within this paper, we introduce and investigate quantitatively the method of Structure-from-Motion (SfM) photogrammetry using high resolution Unmanned Aerial Vehicle (UAV) imagery to accurately model crop trials, from which generation of crop heights can be calculated.

1.4. UAVs in Research

Unmanned Aerial Vehicles (UAVs), also referred to as Unmanned Aerial Systems (UAS), are a growing technology that is rapidly gaining popularity in both the public and scientific communities. UAVs offer a customisable aerial platform from which a variety of sensors can be mounted and flown to collect aerial imagery with very high spatial and temporal resolutions. Advancements in the accuracy, economic efficiency and miniaturisation of many technologies including GPS and computer processors has pushed UAV systems into a cost effective, innovative remote sensing platform.

Of most significance for research applications is the gap which this technology fills in the remote sensing domain. UAVs overcome the restrictions of resolution and cost that often hamper the use of satellite and airborne remote sensing respectively. The wide variety of sensors which can be

mounted and flown over a predetermined area, means an almost endless list of possible applications for this technology.

A review of the literature highlights the wide range of applications UAVs and mounted sensors have been utilised for. For environmental monitoring, examples include modelling of the temporal changes in landslide dynamics [18]; 3D reconstruction of fluvial topography of UK streams [19]; monitoring of rangeland [20,21] and conservation applications such as surveying of habitats and animal numbers [22]. Alternatively, UAVs have been applied in documenting of archaeological sites, where the rapid collection of very high-resolution 3D reconstructions from UAV based methods has been proven useful [23]. In terms of agriculture, UAVs have been used for the monitoring of water status and drought stresses in fruit trees [24]; additionally, collecting multispectral and hyperspectral imagery for use in spectral indices [25] and even chlorophyll fluorescence [26].

1.5. Structure-from-Motion and Crop Modelling

SfM photogrammetry is an emerging method that offers high resolution 3D topographic or structural reconstruction from overlapping imagery [27,28]. Key to SfM methods is the ability to calculate camera position, orientation and scene geometry purely from the set of overlapping images provided, offering a simple processing workflow compared to alternative photogrammetry techniques [29,30]. The simple and easy workflow of SfM for generating 3D digital reconstructions of landscapes or scenes makes it applicable for use a variety of research fields as well as in agricultural crop monitoring.

A number of studies have applied UAV based SfM to modelling crop heights and/or growth over the growing season. Bendig et al. [31,32] applied UAV based SfM methods to model and calculate heights of barley and rice crops in the field. Results showed room for development in the methods and technologies used; comparisons with ground measured heights of barley produced regression coefficients values of 0.55, 0.22 and 0.71 on three different dates. The authors highlight issues with GPS accuracy as a main source of crop height error, as well as suggesting using higher quality cameras for image collection. Ruiz et al. [33] also found the SfM algorithms suffer from errors present in GPS datasets. Ground-based Control Points (GCP) located within the scene are recommended as best-practice for spatial accuracy and minimisation of model error. Turner et al. [34] found GCPs offered a significant improvement in spatial accuracy compared to directly georeferenced imagery using the UAVs on-board GPS. Aasen et al. [35] used hyperspectral imagery collected from a UAV for vegetation monitoring including height. Results from this study were found to be comparable with others (R^2 = 0.7) with a consistent underestimation of plant height by 0.19 m. The authors highlight the fact that the rule has its own issues when it comes to accuracy and therefore may not offer the best source of ground validation. However, as the standard procedure currently in practice, rule measurements still hold a level of importance when proving the validity of UAV based SfM methods.

Image resolution is particularly important for early season crop modelling where the lack of closed canopies impacts on "Crop Surface Model (CSM)" production [36]. Higher resolutions offer a good level of improvement in model accuracy. Willkomm et al. [37] generated models with spatial resolutions of 0.5 cm, with height reconstructions comparable to the other studies discussed (R^2 = 0.75) and point out a tendency of the UAV models to underestimate heights. Interestingly the authors highlight the inability to isolate singular plant details within the model due plant movement during acquisition, likely due to wind. There is a potential that this crop movement, caused by windy conditions, and subsequent loss of some plant structures may be the cause of the underestimation of the model.

The review of relevant literature has shown UAV based SFM is applicable to modelling of plant heights however accuracy of models achieved in these studies highlights improvements are needed. It is clear that a proof of concept has been achieved, however the development of this concept into a working procedure applicable to real world agricultural research is now the next step.

The aim of this study is to produce a highly accurate and repeatable method for collecting crop heights from UAV based Structure from Motion Photogrammetry models as an alternative to current manual rule based phenotyping methods.

The research will involve accuracy assessments and comparisons with alternative technologies, method development and full season testing of the SfM technique. A full quantitative assessment will address the following research questions:

1. How accurate are the models and crop heights generated, compared to the rule method; the existing industry standard?
2. How replicable is the method over the development cycle of wheat crops, particularly between stages GS30 and GS61 (Zadoks Scale); can growth be monitored?
3. Can these methods be applied in crop research and does it offer a better quality of data compared to the rule method?

2. Materials and Methods

2.1. Field Site

The experiment was performed at Rothamsted Research, UK (51°48′34.56″N, 0°21′22.68″W) as a contribution to the 20:20 Wheat Project, where field trials of a wide range of wheat varieties are ongoing [4]. This study used data collected over the Defra-funded WGIN (Wheat Genetic Improvement Network) Diversity Field Experiment conducted at Rothamsted, which is testing the influence of four different nitrogen fertiliser treatments (0, 100, 200, 350 kg N ha^{-1}) on 25 varieties of wheat, with each treatment having three repetitions [38]. Each repetition consists of a plot of wheat comprising a 9 m × 3 m "main plot", and a 2.5 m × 3 m "sampling plot", used for non-destructive and destructive sampling respectively; all plots are separated by 0.5 m uncropped buffer zones and each treatment strip is separated by 5 m buffers that mostly comprise vehicle tracks. The order of varieties is randomised in each strip. Figure 1 shows an example of one strip containing the 25 wheat varieties subject to one of the four nitrogen treatments. The work used data collected over two growing seasons of the diversity experiment (2014 and 2015), with crop rotation resulting in the location of the plots changing between the years but the experimental set-up remained as shown in Figure 1. The 2014 growing season was used for the pilot project, this included collection and comparison of terrestrial laser scans and UAV SfM photogrammetry against the existing rule method in order to compare methods and determine the performance of the UAV method in crop height estimation. The 2015 main study used the UAV method to derive crop height and growth rate over the entire field as well as to confirm the accuracy levels of height estimation over wider areas and more wheat varieties than the pilot project had included.

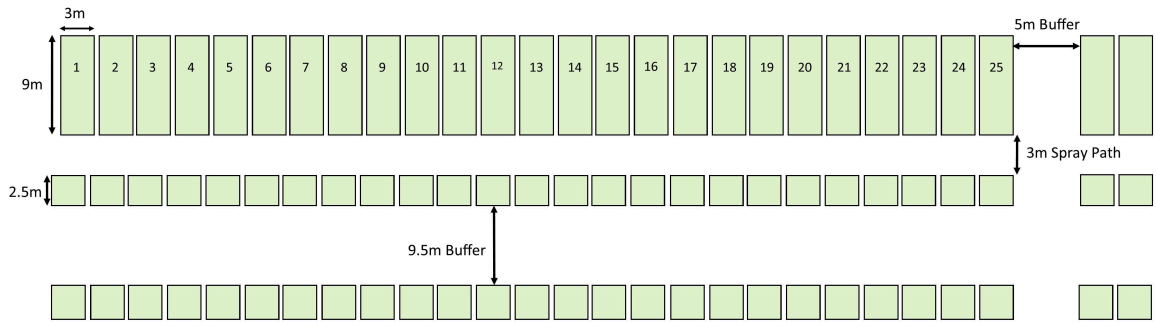

Figure 1. Layout of a single diversity experiment field planting strip, consisting of 25 plots each growing a different wheat cultivar. This layout was repeated 12 times, 3 times for each of the four different nitrogen treatments, and so the field contained 300 plots in total (with each plot consisting of a larger 9 m × 3 m "main plot", and a 2.5 m × 3 m "sampling plot").

For simplicity, N1, N2, N3 and N4 will be used herein to refer to the four different nitrogen fertiliser treatments of 0, 100, 200, 350 kg N ha^{-1} as detailed in Table 1. The 25 different wheat varieties are listed in Table 2 and will from hereon be referred to by the initials codes shown.

Table 1. Details of the four nitrogen fertiliser treatments applied to the diversity field experiment in 2015.

Treatment Code	Total Nitrogen Application (kg N ha^{-1})	Application Dates	Amount of Nitrogen Applied (kg N ha^{-1})
N1	0	-	0
		-	0
		-	0
N2	100	16 March 2015	50
		1 April 2015	50
		30 April 2015	0
N3	200	16 March 2015	50
		1 April 2015	100
		30 April 2015	50
N4	350	16 March 2015	50
		1 April 2015	250
		30 April 2015	50

Table 2. Codes for each cultivar of wheat crop grown in the diversity field experiment.

Cultivar	Code
Avalon	AV
Bonham	BO
Cadenza	CA
Claire	CL
Cocoon	CC
Conqueror	CN
Cordiale	CO
Crusoe	CR
Evoke	EV
Gallant	GA
Hereford	HF
Hereward	HE
Hystar	HY
Istabraq	IS
Malacca	MA
Maris Widgeon	MW
Mercia	ME
Paragon	PA
Riband	RI
Robigus	RO
Skyfall	SY
Stigg	ST
Soissons	SS
Solstice	SL
Xi19	XI

2.2. Pilot Project (2014)

A pilot project in 2014 focused on providing an initial accuracy assessment of UAV based SfM approach to crop height determination, as compared to the alternative method of terrestrial laser scanning (LiDAR). Both were compared to the ground based method currently employed on the diversity experiment and which is standard practice in field phenotyping, i.e., manual measurement using a 2 m rule of five random stems from which the mean plot height is determined. All data were

collected 14–18 July 2014 post-anthesis when the crop were undergoing senescence, so no further crop growth was expected.

2.2.1. UAV SfM Method

To provide data for the UAV SfM approach, a Cinestar Octocopter UAV with a DJI Wookong M flight controller carrying a Sony NEX 7 24.3 megapixel camera was flown over the diversity experiment field at two altitudes (90 m and 40 m), using fixed camera settings and a pre-programmed flight path (Figure 2), and using DJI ground station software. The flight path was designed in order to ensure overlapping imagery of at least 60% side overlap and 80% forward overlap; these values were decided on after consultation of existing literature [32,39,40], as well as the Agisoft Photoscan Software manual [41] (Table 3).

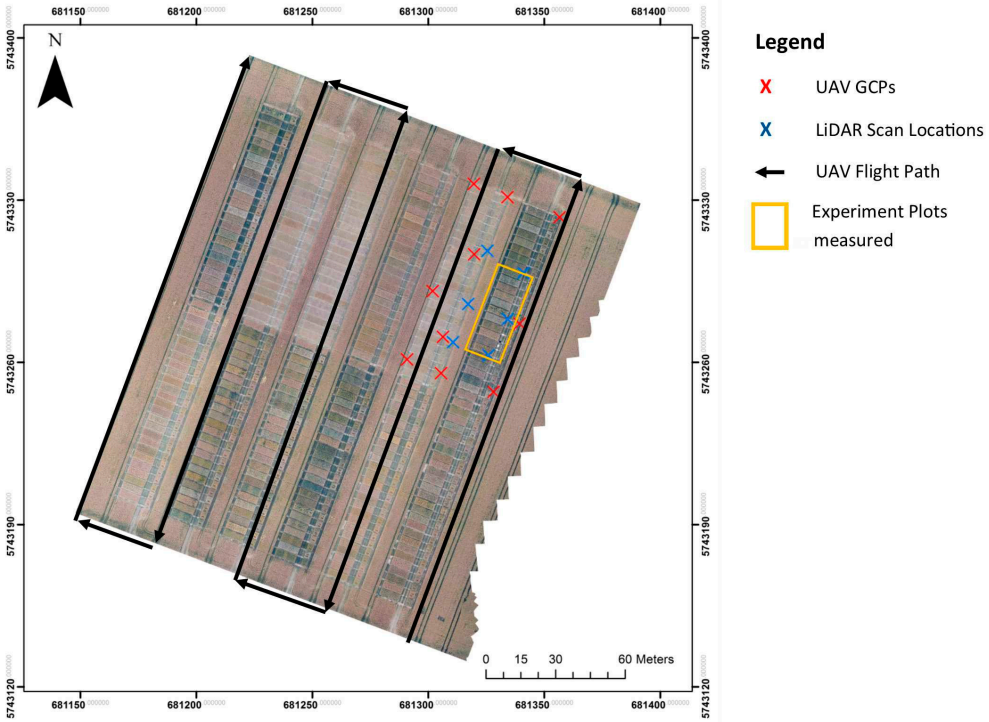

Figure 2. Orthomosaic of the 2014 field, displaying the location of Ground Control Points (GCP), LiDAR scan targets, the UAV flight path and the 10 experimental plots measured for this study. Coordinates are displayed in WGS 1984 Coordinate System.

Table 3. Camera settings and image parameters used for the two data collection flights made during 2014.

Altitude (m)	Aperture	Focal Length	ISO	Shutter Speed	Image Resolution (cm/Pixel)	Image Format
90	f/5.6	14	100	Auto	1.4	JPEG
40	f/4.5	14	100	Auto	0.7	JPEG

The pilot project used only 10 plots of the full diversity field experiment and a set of Ground Control Points (GCPs) consisting of ten 50 cm × 50 cm numbered acrylic panels which were placed evenly across this target area prior to all data collection (Figure 2). The GCP locations were recorded using a differential Global Positioning System (dGPS, Trimble Geo 7, Sunnyvale, CA, USA) to provide sub-centimetre locational precision. Identification of the GCPs in the imagery later allowed for the re-projection of the image mosaic and 3D models into a real-world coordinate system.

Processing of the individual images into an image orthomosaic and Digital Surface Model (DSM) was performed in Agisoft Photoscan Pro (version 1.2.4) [41] (Figure 3), with different models generated using different processing settings and different subsets of the full image database, such as altitude, in order to assess the impact of these on crop height retrieval accuracy. Table 4 provides a summary of the parameters used for the models generated.

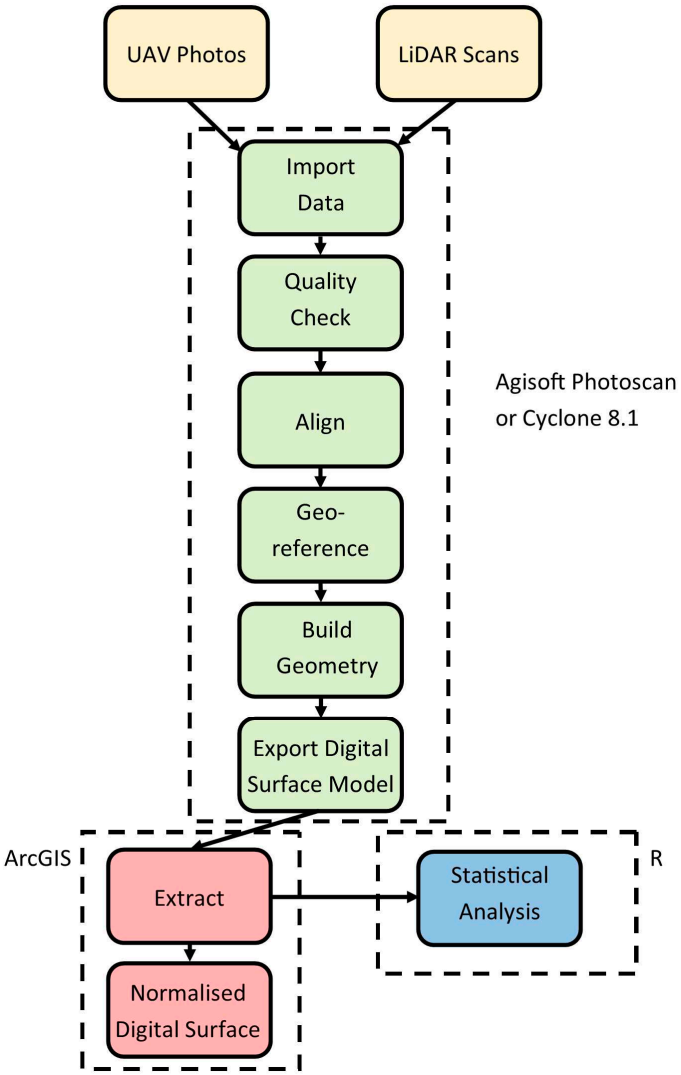

Figure 3. Workflow for processing the collected UAV imagery and Terrestrial LiDAR point clouds into the normalised Digital Surface Model.

Table 4. Parameters of the UAV flights and Agisoft Photoscan processing used in the 2014 Pilot Study. Model resolution is the reported model resolution provide by Agisoft Photoscan.

Model	Altitude (m)	Alignment Accuracy	Dense Cloud Quality	Depth Filtering	Model Resolution (cm/ Pixel)	Model Reference
1	90	High	Medium	Aggressive	2.0	UAV90A
2	90 and 40 combined	High	Medium	Aggressive	1.7	UAV90+40A
3	40	High	Medium	Aggressive	1.0	UAV40A
4	40	High	Medium	Mild	1.0	UAV40M

Review of relevant literature pointed to some disparity in the terminology used to describe the different computed 3D models created in SfM processing. One such example is the use of Crop

Surface Model (CSM), for which Bendig et al. [31,32] describes as the absolute height of crop canopies. Geipel et al. [36], in comparison define a CSM as the difference between the Digital Terrain Model (DTM) and DEM. To prevent confusion and ambiguity, terminology in this article will use definitions as set out by Granshaw [42]. The three model types created within this study, as shown in Figure 4, are Digital Elevation Models (DEM), Digital Surface Models (DSM) and normalised Digital Surface Models (nDSM), definitions are provided in Table 5. It should be noted that the final output from Agisoft Photoscan is what it calls a DEM, this is technically a DSM as it includes both the scene features and underlying topography captured in the imagery although application of depth filtering in processing may remove some top surface features which means use of depth filtering should be acknowledged when assuming a model is a DSM.

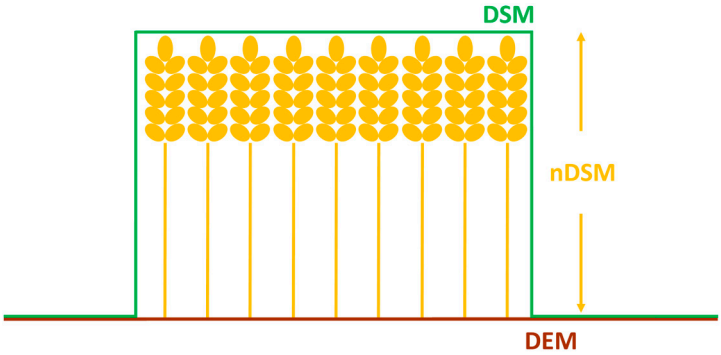

Figure 4. Visual representation of the Digital Surface Model (DSM), normalised Digital Surface Model (nDSM) and Digital Elevation Model (DEM).

Table 5. Definitions of types of models generated in this study, based on definitions offered by Granshaw [42].

Model Name	Abbreviation	Description
Digital Elevation Model	DEM	Model of the underlying field topography without features.
Digital Surface Model	DSM	Combined model of the underlying topography and field features e.g., crops.
Normalised Digital Surface Model	nDSM	Model of field features only (crop heights).

A key step in the production of a final nDSM is the removal of underlying field topography, performed using Equation (1), in order to isolate the pure crop heights.

$$\text{nDSM} = \text{DSM} - \text{DEM} \quad (1)$$

where DSM is the final output model from Agisoft Photoscan Pro and DEM is the underlying field topography, created through extraction of bare ground heights located in the unplanted buffer zones between the plots throughout the field. These bare ground heights were then extrapolated into a DEM. Investigation was also carried out to assess a potentially more universal method for use where large buffer zones are not included in the field layout, such as those in commercial fields. This alternative method involved generating a DEM from the field when no crops were present in order to measure the bare ground.

2.2.2. Terrestrial LiDAR Method

Alongside the UAV data, a Leica HDS6100 Terrestrial LiDAR was used to collect LiDAR point clouds of nine plots, this system providing a very high 5 mm measurement precision but with the disadvantage of a relatively time-consuming measurement procedure compared to the UAV when multiple scans from different directions are required. Here we used six scans from different positions

around the plots (Figure 2) to ensure both a highly dense point cloud and minimal shadowing. Scanner settings are detailed in Table 6, with six Leica "Tip and Turn" targets placed within the scan area whose location was also measured with dGPS and whose record in the scans were used for inter-scan registration and point cloud geo-referencing in the Leica Cyclone 8.1 software [43]. Point clouds were generated from first return pulses and after registration and geo-location, were analysed and crop heights extracted (Figure 3).

Table 6. LiDAR settings used during 2014 study.

Scanner Parameter	Settings Used
Laser Poser	High
Scan Resolution	Super High
Vertical Extent	25°–180°
Horizontal Extent	Manually selected depending on scan.

2.3. Main Study (2015)

The objective of the Main study was to apply the UAV based crop height retrieval method developed in the 2014 Pilot at the full field scale and over the whole growing season—using it to assess the crop growth rate of the different varieties and nitrogen fertiliser application levels of the diversity experiment. During this study, ground-based (rule) measures of the height of all 300 plots were collected on two occasions (18 June 2015 and 17 July 2015) for comparison to the UAV-derived crop height measures; a sub sample of 100 plots was also measured by rule on 22 May 2015.

UAV SfM Method

Image collection flights were conducted over the full diversity experiment field on a regular basis, weather and equipment permitting between March and July 2015. Flight altitude was kept at 45 m on the basis of the findings of the pilot project, and the same flight plan used each time (Figure 5). Camera settings were kept as consistent as possible, though changes were needed occasionally to allow for changing illumination conditions as well as a change in lens due to damage (Table 7). These changes had not detrimental effect on final model resolutions. Between 21 March and 21 April 2015 no flights were conducted due to technical problems with the UAV. Thirty two GCPs were located in the field (Figure 5), evenly spread throughout and with their location measured with dGPS as before. Images were processed using Agisoft Photoscan under the same workflow as Figure 3. There were two changes to processing settings however; investigation of high and ultra-high dense cloud quality settings found DSM quality could be increased when using high quality but ultra-high introduced very high levels of noise, as such all models in the 2015 study were processed with the high setting. The second change was due to updates to the Photoscan software which allowed for depth filtering to be disabled on all models used for monitoring growth. This was done to reduce the smoothing of features such as the tops of the wheat crops in the models. Table 8 details the key model parameters.

Table 7. Camera settings and image parameters for each flight used in the 2015 study.

Date	Focal Length	Aperture	ISO	Shutter Speed	Image Resolution (cm/Pixel)
19 March 2015	20	f/4	Auto	1/1000	0.9
2 April 2015	18	f/4	Auto	1/1600	0.9
14 April 2015	18	f/4	Auto	1/1600	0.9
21 April 2015	15	f/4	Auto	1/1600	0.9
21 May 2015	17	f/4	Auto	1/1600	0.9
4 June 2015	18	f/4	Auto	1/1600	0.9
17 June 2015	20	f/4	Auto	1/1600	0.9
26 June 2015	20	f/4	Auto	1/1600	0.9
6 July 2015	20	f/4	Auto	1/1600	0.9
20 July 2015	20	f/4	Auto	1/1000	0.9

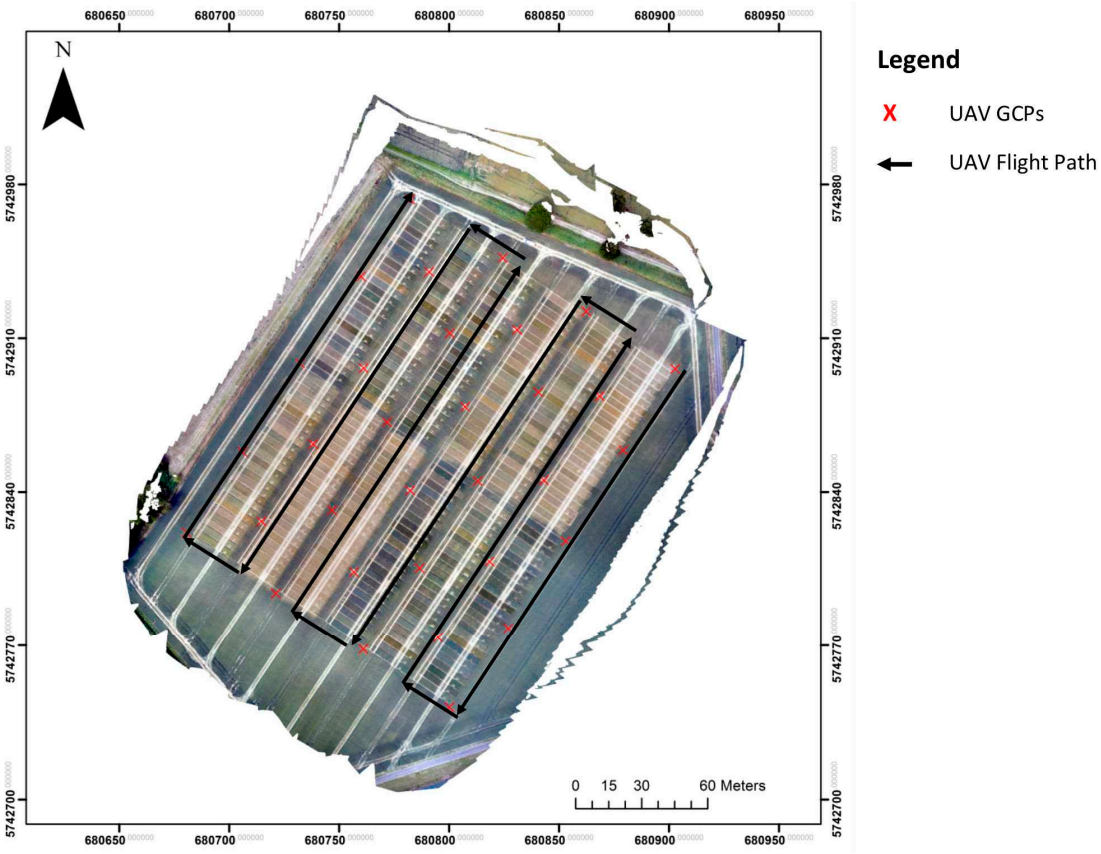

Figure 5. Orthomosaic of the 2015 field, displaying the location of Ground Control Points (GCP) and the UAV flight path used. Coordinates are displayed in WGS 1984 Coordinate System.

Table 8. Agisoft processing parameters used in the 2015 study. The model resolution provided is the resolution reported by Agisoft Photoscan.

Alignment Accuracy	Dense Cloud Quality	Depth Filtering	Model Resolution (cm/Pixel)
High	High	Disabled	1

As a potential alternative to using the heights of the buffer zones as a means to create a bare ground DEM over this much larger area than that used in the 2014 Pilot study, flights were also conducted in 2015 after harvest (but before ploughing) on 25 September 2015 to enable a bare ground DEM to be derived using imagery of the non-cropped field. As this was post-harvest some crop stubble was still remaining in the field.

After creating and normalising the models for field topography, a plot map was created before crop heights for each plot were extracted and mean heights calculated. Plot borders were created in ArcGIS using the experimental layout dimensions (Figure 1). Some actual field plots did not fit the layout plan exactly and so were shifted and rotated manually as necessary to the right position. To prevent plot edge effect influencing calculations, plots were shrunk by 50 cm on each edge using an ArcGIS buffer tool (Figure 6). This value (50 cm) was arbitrarily chosen for this experiment. This approach will require automation in the future for experiments consisting of thousands of plots, where the outlining of individual plots manually is very time consuming.

Initial analyses highlighted an issue with some plots displaying mean heights much lower than the corresponding ground-based measures taken with the measuring rule. Examination of the original imagery indicated that, similar to the findings of [36], a lack of canopy development and stem population density in the unfertilised (N1) plots compared to the fertilised plots was the cause.

The reduced canopy coverage increased the proportion of pixels showing either lower level plant structures or even patches of bare ground between plants (Figure 7). In order to remove this effect, all future mean plot heights were generated from the 99th percentile, rather than the total mean, such that the top height of the plants were reported, as is the case with the current ground-based method. This method was chosen over standard mean or median as it was best at isolating the top photosynthetic tissue of each plant, and avoiding occasional contaminating individual rogue or anomalous plants, which is required in order to obtain true plant height as defined in Section 1.3.

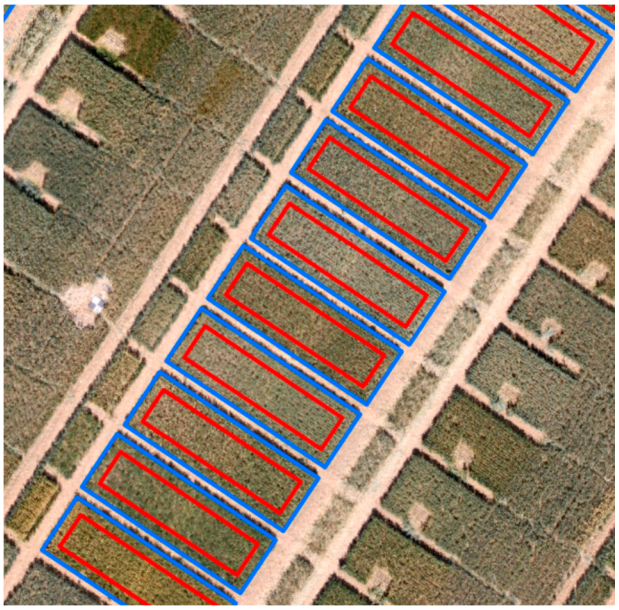

Figure 6. Plot borders before (**blue**) and after (**red**) buffering isolating each plot within the field in order to extract heights.

(**a**) (**b**)

Figure 7. Imagery collected by the UAV flying at 45 m height of an unfertilised (N1) treatment plot (**a**) compared to an N4 (350 kg·ha^{-1} fertiliser application) treatment plot (**b**). Mercia wheat cultivar shown in both cases.

3. Results

3.1. Pilot Project Results

Results from the 2014 Pilot study are focused on a comparison of the different UAV-derived and LiDAR-derived nDSMs with those from the standard ground-based method (Figure 8). All linear best fits between the UAV and LiDAR models and the ground-based measures heights show intercepts close to 0, but with slopes varying from close to 1.0 (LiDAR and UAV40M) to 0.73 (UAV9040A). The LiDAR and lower altitude UAV-derived results also show the highest regression coefficients with the ground-based data (R^2 =0.97 for LiDAR and R^2 = 0.99 for UAV40M). Root Mean Squared Error

(RMSE) statistics indicate both these methods are providing crop height retrievals to within around 3 cm of the ground-based measures. However, there are some biases shown, with all the UAV-derived nDSMs underestimating height to some degree (by 24 mm to 158 mm), with the lowest altitude imagery showing the lowest bias. LiDAR biases are by comparison only 4 mm.

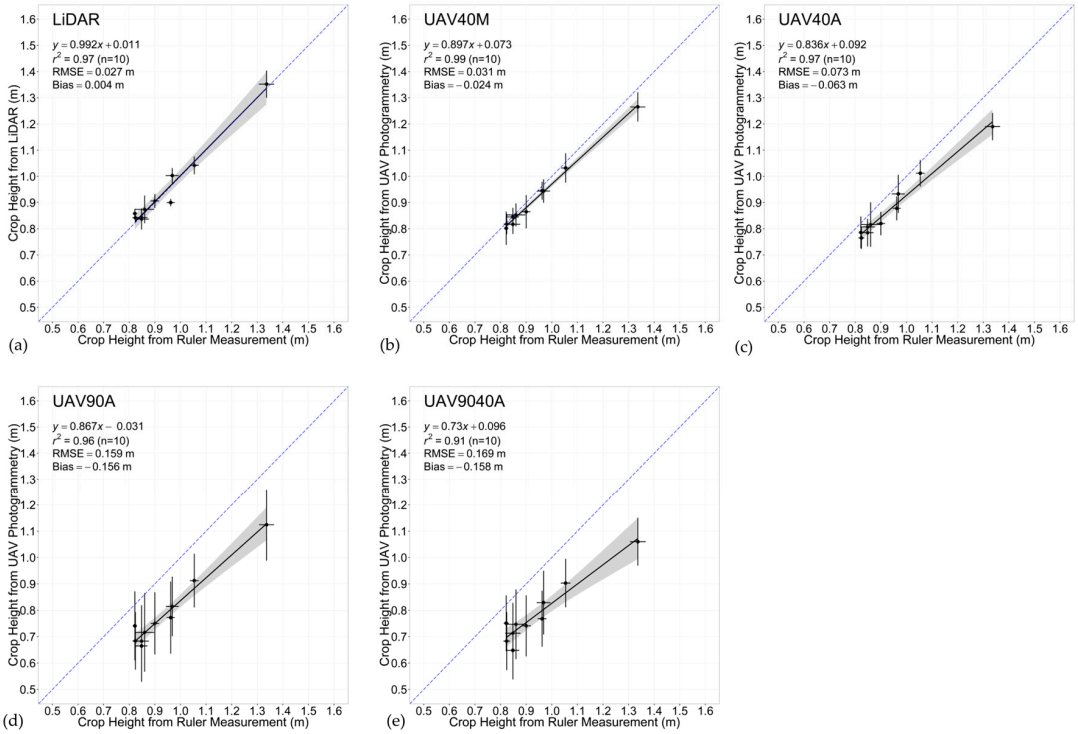

Figure 8. Comparison of crop heights derived from (**a**) LiDAR and (**b**–**e**) the various UAV-based approaches detailed in Table 4 to those from the ground-based (rule) method for each of the ten plots measured during the 2014 Pilot study. Blue dashed line indicates 1:1 slope.

The results show both the LiDAR and UAV based SfM techniques are fully capable of recreating accurate 3D models and subsequent crop heights of wheat crop trials in the field.

For the UAV results, lower altitudes produced significantly more accurate crop heights, due to the higher image ground resolution achieved at the lower altitude. There was a clear advantage to using "mild depth filtering" during processing in order to achieve greater crop height accuracy, likely due to the reduction in "smoothing" of the model allowing for more of the small plant features of interest to remain during the depth filtering step of model processing.

3.2. Main Study Results

3.2.1. "Bare Ground" DEM Selection

Due to its importance in producing the final nDSMs, analysis of two methods for producing the bare ground DEMs was performed. nDSMs were produced using the same "buffer zone height" approach used in the 2014 Pilot, and the alternative "post-harvest DEM" based on a bare ground DEM derived from post-harvest imagery. The resulting maps of crop height were then compared to the corresponding ground-based measures, with both sets of results showing R^2 values of >0.93 (Figure 9). However, the RMSE statistics indicate that use of the DEM based on the buffer zone heights produces crop heights with reduced levels of error compared to that based on the post-harvest imagery. This is likely due to any bias present in the "buffer zone" DEM is also present in the model and crop heights being taken at the same time, therefore this bias is cancelled out, whereas in the case of the post-harvest DEM, any bias present, including the potential impact of the post-harvest stubble will not be cancelled

out when plant heights are extracted. All subsequent nDSMs in this study were generated using the "buffer zone" DEM approach.

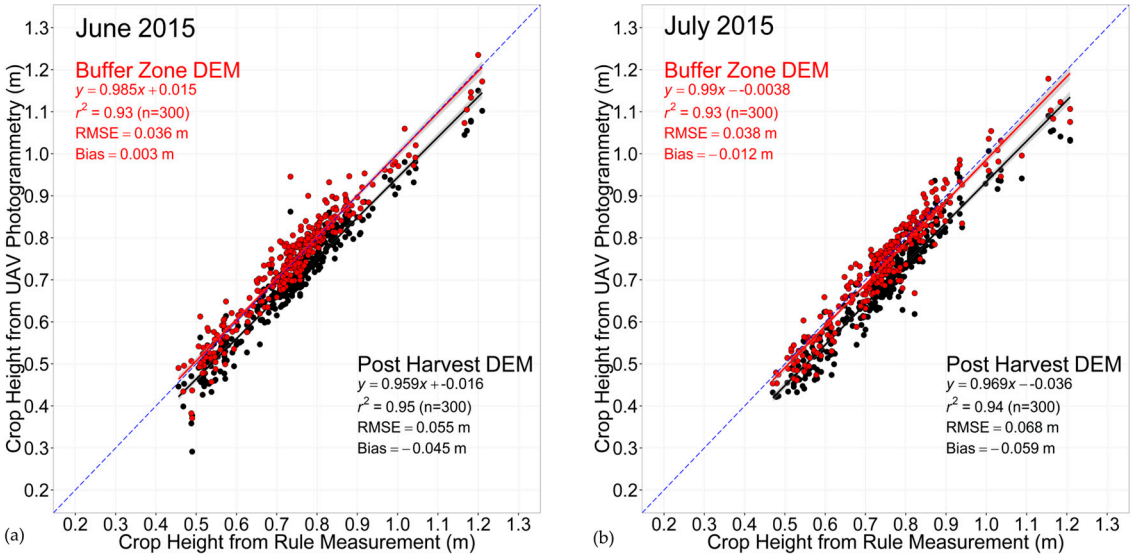

Figure 9. Comparison of "buffer zone" (**red**) and "post-harvest" (**black**) DEM generated crop heights for June (**a**) and July (**b**) 2015. The blue dashed line indicates a 1:1 slope.

3.2.2. Accuracy Assessments

In addition to the accuracy assessment conducted in the Pilot Study during the crop senescent stage, three further similar assessments were conducted in May, June and July of 2015 at different periods during the crop growing cycle (Figure 10). For these accuracy assessments, the mean height of the three replicates measured from the UAV models was compared to the rule measured mean heights.

The comparison between UAV-derived and ground-based crop heights shown in Figure 10 indicates consistently high levels of accuracy, most particularly in the June and July assessments. May aerial measurements show a much more significant underestimation of height compared to July, and June shows some very small overestimation bias (3 mm). The lower accuracy achieved in the May assessment is thought to be caused by the earlier development phase of the varieties where canopies were not fully complete, an influence discussed previously in Section 2.3. Comparison between nitrogen treatments (Table 9) shows the N1 treatment generally has lower accuracy levels, again likely due to the influence of reduced canopy development in these plots.

Table 9. Accuracy Assessment results of three different comparisons of rule measured and UAV measured heights. The results are grouped by the four nitrogen treatments applied within the diversity field experiment.

Model	Treatment	RMSE (m)	BIAS (m)	R2
May	N1 (0 kg·hectare^{-1})	0.094	−0.089	0.76 (n = 25)
	N2 (100 kg·hectare^{-1})	0.099	−0.096	0.85 (n = 25)
	N3 (200 kg·hectare^{-1})	0.063	−0.051	0.52 (n = 25)
	N4 (350 kg·hectare^{-1})	0.026	−0.02	0.91 (n = 25)
June	N1 (0 kg·hectare^{-1})	0.028	−0.007	0.83 (n = 25)
	N2 (100 kg·hectare^{-1})	0.015	0	0.97 (n = 25)
	N3 (200 kg·hectare^{-1})	0.020	0.007	0.99 (n = 25)
	N4 (350 kg·hectare^{-1})	0.024	0.013	0.97 (n = 25)
July	N1 (0 kg·hectare^{-1})	0.033	−0.026	0.89 (n = 25)
	N2 (100 kg·hectare^{-1})	0.022	−0.018	0.98 (n = 25)
	N3 (200 kg·hectare^{-1})	0.021	−0.009	0.98 (n = 25)
	N4 (350 kg·hectare^{-1})	0.020	0.007	0.96 (n = 25)

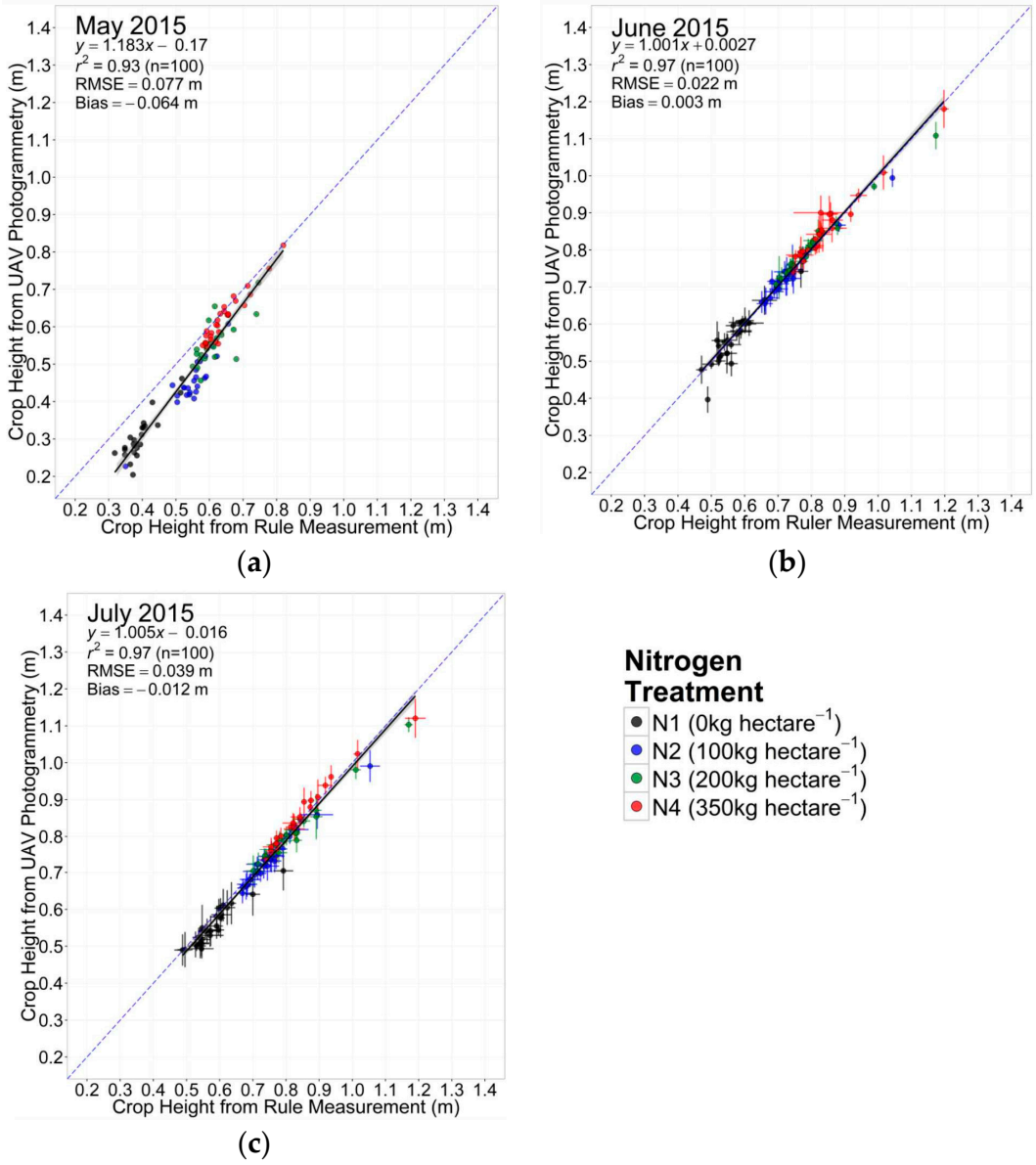

Figure 10. The 2015 accuracy assessments of UAV-derived mean crop heights made against standard ground-based rule measures performed as per Section 2.2). Accuracy assessment covered the four nitrogen treatments in: (**a**) May 2015 where the crops were still growing; and (**b**) June 2015; and (**c**) July 2015 when the crops were post anthesis and no longer expected to grow. The error bars represent the standard deviation of crop height between the three replicates from each cultivar and treatment. The blue dashed line indicates a 1:1 slope.

The replicate standard deviation shown by the error bars show a small amount of variation between replicates as would be expected in a field based experiment such as this, importantly this variation is displayed both in the heights measured by the rule and by the UAV model. The June assessment shows one plot has noticeably larger variation in the rule measured heights compared with the UAV heights for the same plot.

3.2.3. Plant Height

A key objective of the Main Study was to demonstrate the capability to assess crop growth and growth rates over the growing season.

All processed models show consistent patterns with the rule measured heights except for one error in plot 298, Maris Widgeon, in the 4 June 2016 nDSM. On examination this plot showed the presence of noise in the model located above plot 298 resulting in larger than expected heights for this plot. The sources of this noise is unknown and has not impacted on any other plots within this nDSM or other nDSMs. This erroneous plot was omitted from the height and growth rate calculations from this 4 June nDSM, using only data from the other two Maris Widgeon N1 plots.

Figure 11 shows the crop height measures obtained from imagery collected from March 2015 to July 2015, which indicate that the predominant growth in all varieties occurs from mid-April to mid-June. After this point some varieties show a levelling off in crop height suggesting no further growth occurs whilst other varieties and particularly crops grown in the N1 treatment show a decline in height after mid-June.

Overall, there is relatively little variation between the heights of replicates (as depicted by the error bars of Figure 11), similar to the levels seen in the accuracy assessments (Figure 10).

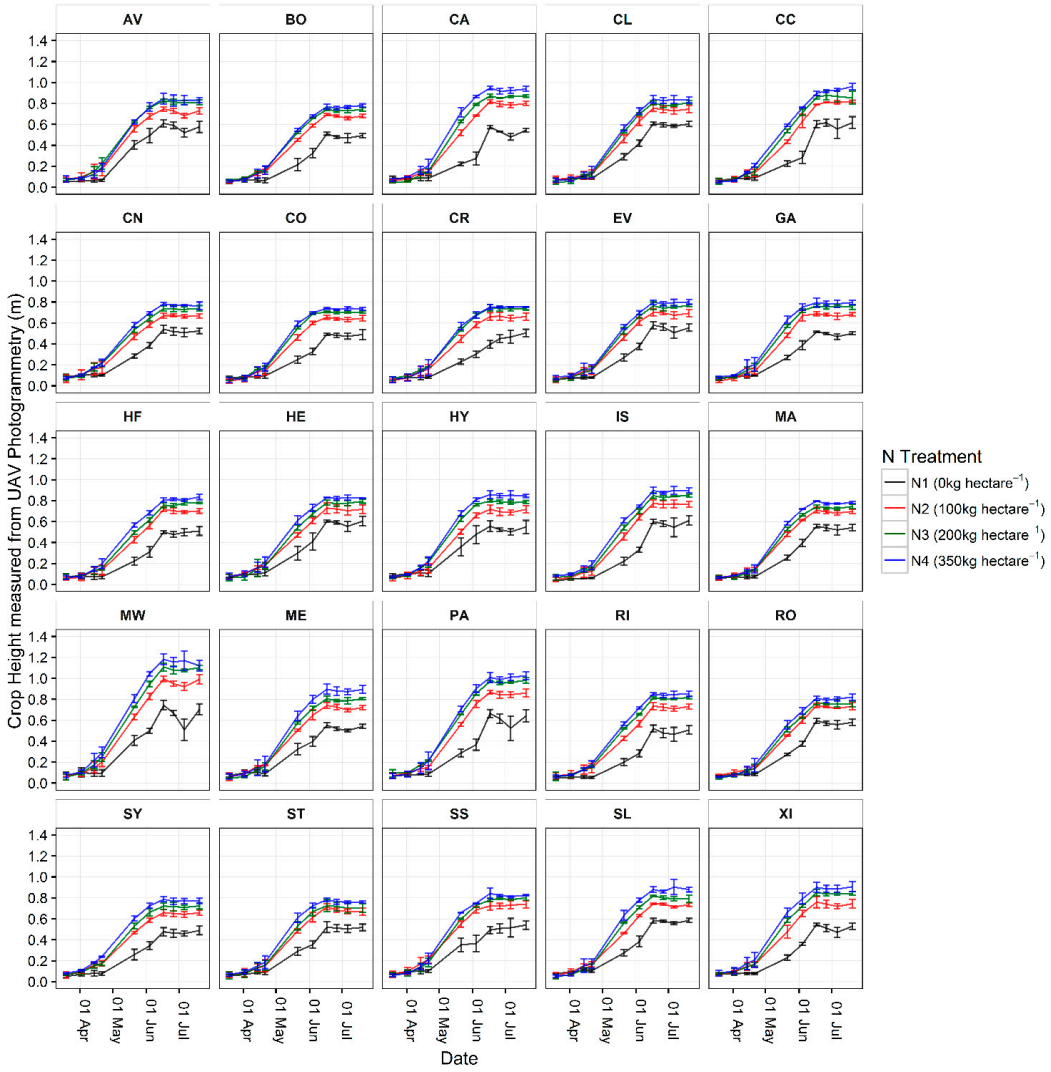

Figure 11. Changes in average crop height of the wheat varieties at the four N treatments. Variation in crop height between replicate plots is displayed by error bars. Crop varieties are referred to by their code as set out in Table 2 and all data are the means of three replicate plots, except Maris Widgeon N1 on the 4 June 2015 which is the mean of two replicates due to plot 298 being omitted because of noise in the model.

3.2.4. Growth Rate

Once the change in crop height was calculated with confidence, crop growth rate was assessed by dividing height change by the date interval to examine how growth rate changes between nitrogen treatments.

Figure 12 presents the growth rate of the different crop varieties and nitrogen treatments. As with crop height data shown in Figure 11, the replicate means and standard deviation of growth for each replicate set is show. Results show a common bell shaped pattern in growth rate between mid-April and mid-June, corresponding to the main period of crop height increase seen in Figure 11. This trend is less apparent in the N1 treatments, which tend to show lower growth rates until June where there is a spike in growth rates displayed by most varieties in the N1 treatments.

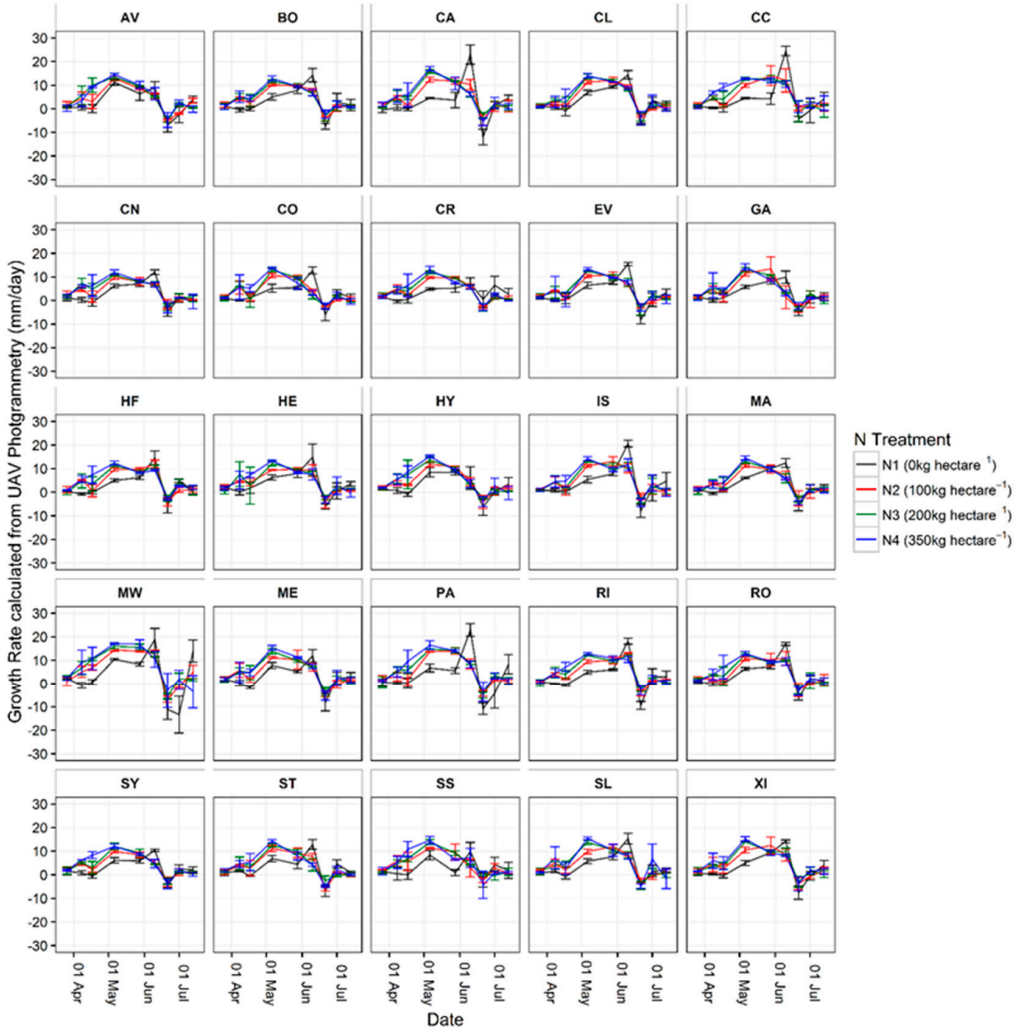

Figure 12. Mean growth rate inferred from height increase of wheat varieties subjected to different nitrogen fertiliser treatments. Growth rate is calculated from the data of Figure 12 and the time interval between the dates of each normalised digital surface model. Crop varieties are referred to by their code as set out in Table 2 and all data are the means of three replicate plots, except Maris Widgeon N1 on the 4 June 2015 which is the mean of two replicates due to plot 298 being omitted because of noise in the model.

All varieties and treatments show a drop into negative growth rates in mid-June. One possible explanation is due to the ears of the plants bending over, sometimes referred to as necking, as the plant matures. Another potential source of the negative growth rate is due to decreasing plant water content

from around 80% when the plants are fully green to <20% at harvest. This decline in water will lead to some level of cell shrinkage and subsequently decreasing plant height after mid-June. It is likely a mix of these two reasons explain the negative growth rate displayed by the crops in mid-June.

3.2.5. Spatial Mapping

The current standard method of using 5 point based rule measures of crop height for each plot offers very little in terms of measuring spatial variability, particularly within individual plots where growing conditions may cause variations in height. The nDSMs produced from the UAV method in this study not only offer measures of height but also visual maps of crop height variability on a field scale (Figure 13), comparing plots side by side throughout crop development. In addition, due to the very high resolution of the models (1cm), variability of crop heights within each plot can be assessed as shown by Figure 14 which even shows areas where the crops have been unable to grow leaving a hole within the plot. This is something unlikely to be noticed from ground based assessments of the fields, particularly when crops are more developed.

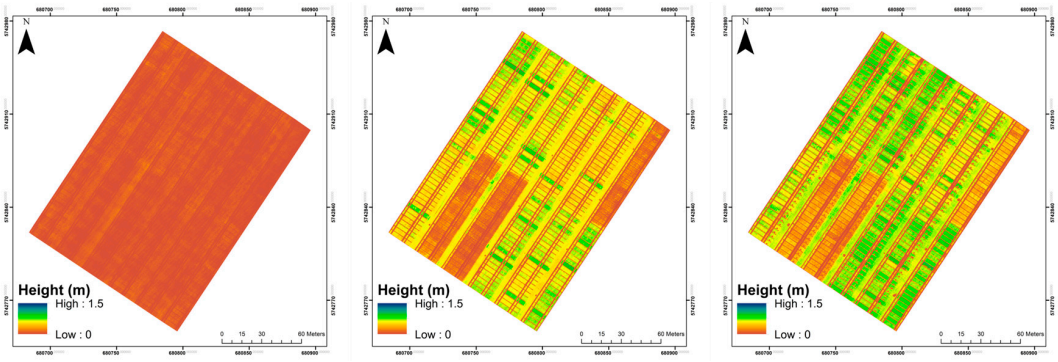

Figure 13. Normalised Digital Surface Models (nDSM) for three different wheat development stages captured on the 14 April 2015, 4 June 2015 and 6 July 2015 respectively. Clearly visible in the middle and right-hand figures are the 0 Kg·hectare^{-1} nitrogen treatment strips where crop height has been noticeably stunted compared to surrounding plots. Coordinates are displayed in WGS 1984 Coordinate System.

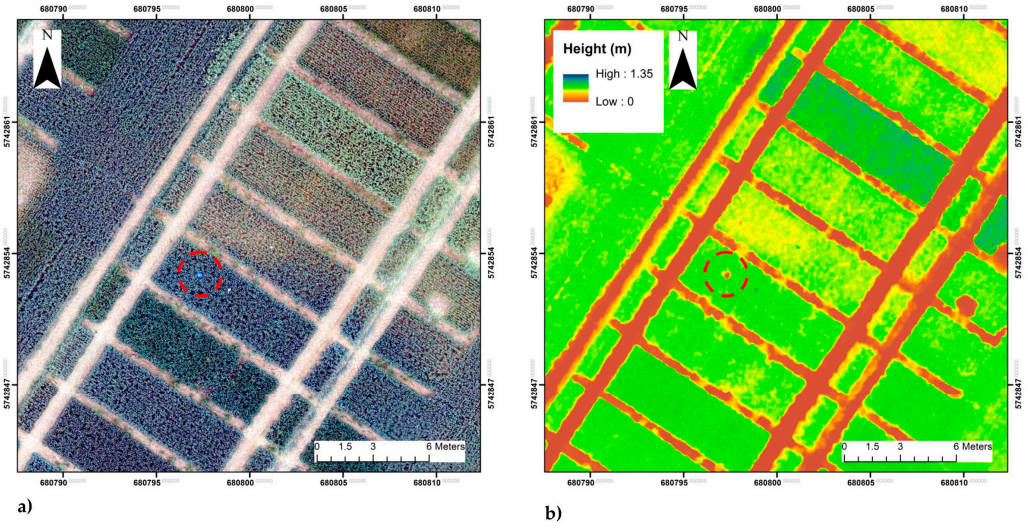

Figure 14. Side-by-side comparison of different cultivar plots in the N4 Treatment highlight the within-plot variability mapping achieved through the UAV based SfM technique. A hole (red circle) in the one of the plots is hard to make out in the orthomosaic (**a**) whilst being clearly visible in the nDSM (**b**). Data captured on 17 June 2015 and coordinates are displayed in WGS 1984 Coordinate System.

3.3. Nitrogen Application and Cultivar Responses

A key focus of this study was to produce a practical high throughput crop measurement system that provides valuable data to crop researchers for use in on-going crop development experiments. The experimental field used in this study was assessing how different wheat varieties were influenced by the quantity of nitrogen (N) fertiliser applied through the season.

The results in Figure 15 show the pattern of crop height increase through the season for each cultivar and the influence of N fertilization. Crop height increases rapidly at the beginning of April in a recognised wheat crop growth phase known as the start of stem elongation (GS30–GS61). The start and rate of stem elongation is earlier and at a greater rate, respectively at the higher N inputs. Maximal height is achieved in mid-June irrespective of the N-treatment but is noticeably lower at the zero N treatment (N1). Individual varieties are characterised by their mature height with Maris Widgeon being notable as a taller cultivar, reflecting the origin of this cultivar as being bred prior to the incorporation of dwarfing alleles. This tall cultivar is very susceptible to wind and rain and may easily lodge (fall over), reflected in the variable data obtained for this cultivar and the apparent decrease seen in some cases during the June period. Plots recover from mild lodging but in severe cases the flattening is irreversible.

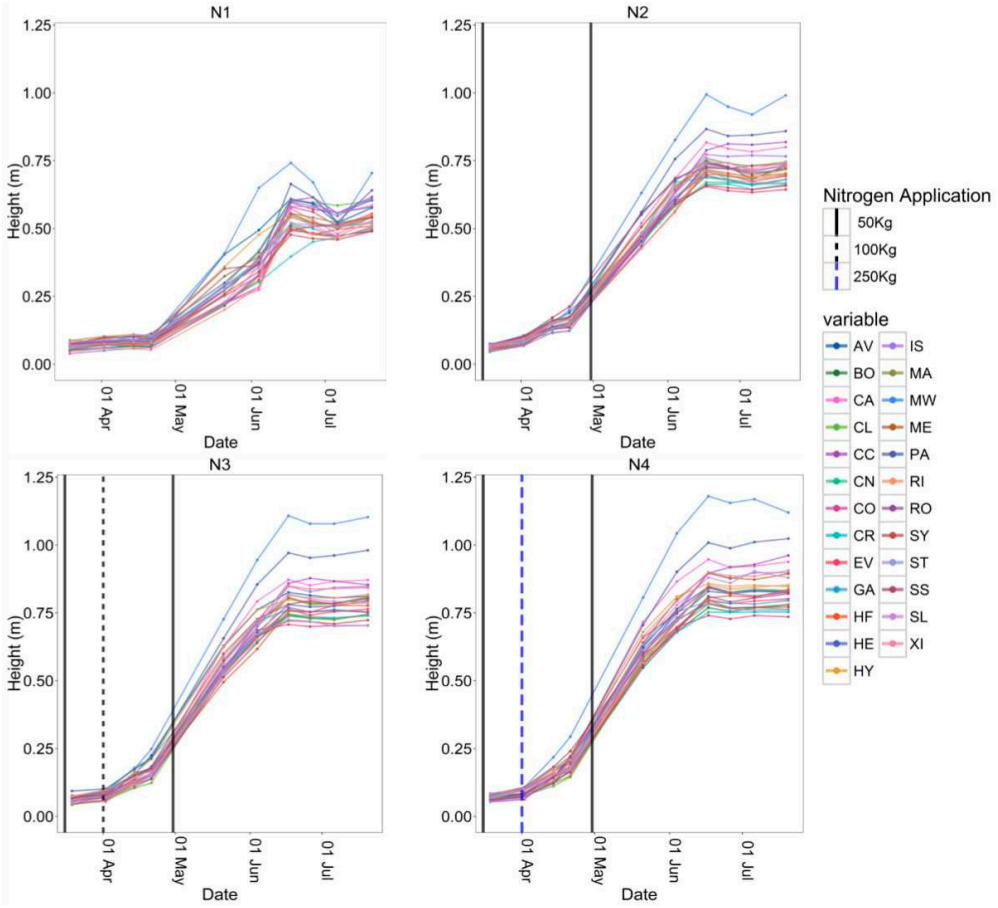

Figure 15. Comparison of crop height over the season grouped by nitrogen treatment. Vertical lines in each figure represent the date and quantity of nitrogen applied to plots for each treatment. All data represent the means of three replicates.

4. Discussion

This study has provided a quantifiable assessment of Unmanned Aerial Vehicle (UAV) based Structure from Motion (SfM) Photogrammetry for deriving accurate measurements of crop height

and crop growth rate, in this case to support field phenotyping efforts of 25 wheat varieties grown under four different nitrogen fertiliser treatments. The method presented is relatively straightforward, easily repeatable, and time and cost efficient in comparison to the terrestrial LiDAR and currently used rule method also investigated in this study.

In terms of accuracy, the data produced provide good agreement with the currently applied procedure of manual measurement with a rule (R2 = $\geq$0.93, Root Mean Squared Error (RMSE) = $\leq$0.077 m) but this approach is more consistent and spatially extensive, reducing user error associated with the ruler measurement [35,44]. Assessment of model derived crop heights from a highly accurate (5 mm) Terrestrial LiDAR (R2 = 0.97, RMSE = 0.027 m) and the best UAV model (R2 = 0.99, RMSE = 0.03 m) shows both system's ability to produce highly accurate results; however extremely high costs and poor time efficiency of the LiDAR due to the high number of individual scans required, severely lower the suitability of LiDAR for this application. The UAV method was found to often underestimate crop heights, as discussed by previous studies [35,37], but overall the results showed an improvement in accuracy compared to similar studies [31,32,45], even when the method was applied over a significantly larger number of trial plots (300).

Collection of crop heights over the growing season has proven the ability of this method to collect valuable phenotypic data at development stages between GS30 and GS61 (Zadoks Scale), and is in agreement with literature [31,46]. A number of field based variables were identified from the study as key influencers on final results; namely canopy structure and density were found to impact on model height accuracy both in early growth stages and in crops grown under nutrient deficient conditions, as also discussed by [36]. The repetition of height measurements from the UAV method allowed crop growth rates to be calculated and assessed. The main results of this study were in agreement with the literature which defines the main period of UK wheat crop growth in terms of height gain between early-April and mid-June [14].

As a high-throughput field phenotyping system, this study has demonstrated that UAV SfM is capable of collecting quality, high volume field based phenotypic data. Comparison to the LiDAR shows the UAV method is able to achieve the same high level of accuracy whilst bettering the LiDAR in terms of time and cost efficiency. Alternative high-throughput platforms that have been developed and investigated further show the value of a system for rapid monitoring of canopy dynamics; such as the Field Scanalyzer [47] as well as movable tractor based systems [48,49]. Advantages of these systems over the UAV focus strongly on the lack of weight restrictions, allowing for multiple sensors to be used to collect very high resolution data from multiple sensors simultaneously. However, these systems are limited in their application over larger areas, or across different field locations, something the UAV is better suited to. The tractor based system proposed by Comar et al. [49], was able to sample ~100 plots per hour, which equates to 1000 plots within three days assuming 4–5 h of measuring per day. The UAV method was able to cover 300 plots within a single flight of maximum 15 min, indicating coverage of 1000 plots could be achieved in less than an hour. Clearly there is a trade-off between the systems discussed here as well as other alternatives. The choice of which system is most suitable will be dependent on the data required, the time frame available and the area of coverage needed.

Whilst the method developed in this study has been shown to produce quality results over the temporal scale of a growing season, there is still room for improvement in the understanding of SfM photogrammetry dependencies. For example, in relation to the camera viewing angle, James and Robson [29] found the inclusion of oblique imagery into a NADIR image data set can further improve 3D model accuracy. In this study, software settings were also found to be influential on accuracy of model outputs, therefore in future these should be carefully selected and accurately reported in order to facilitate further advances in UAV based SfM methods and in the accuracy of results. The use of NIR imagery instead of RGB is also an area of interest, as the increased contrast between plant and soil offered by NIR imagery may improve model processing; a potential solution to the negative influence

of decreased canopy structure on model derived heights as shown by the May accuracy assessment results (Figure 10) and also discussed in the literature [36].

5. Conclusions

The work presented in this paper develops a rapid and accurate method for collecting in-field measurements of crop height using Unmanned Aerial Vehicle (UAV) based remote sensing. The UAV method developed utilises very high resolution UAV imagery and a Structure from Motion photogrammetry workflow to produce 3D topographic reconstructions of the crop trial field. Accuracy assessments of the UAV derived crop heights showed the method was able to produce measures of height comparable in accuracy to those measured by the existing manual, rule based method (R^2 = $\geq$0.92, Root Mean Squared Error (RMSE) = $\leq$0.07m). The very high spatial resolution of the UAV derived data allows for assessment of spatial variability in crop height at both the field and plot scale. UAV flight campaigns throughout the season allowed for the monitoring of changes in crop height as well as the calculation of growth rate.

Future work will look to increase the temporal resolution of the methods in order to provide a more complete picture of this phenotypic trait throughout the development stages of the different cultivars. It will also look to develop methods using other imaging equipment such as multi-spectral [50–52], hyper-spectral [35] and thermal cameras [53,54] to provide information beyond just plant height and growth rate. This should help to open up the opportunity to collect a more complete set of crop phenotype metrics at a spatial and temporal resolution usually unavailable to plant scientists, offering greater insights into varieties behaviours and adaptability under different growing conditions.

Overall, UAV SfM has the potential to become a valuable tool for rapid high-throughput in-field phenotyping of crop heights at very high resolution and accuracy for use in crop trials or more general agricultural applications.

Acknowledgments: This project forms part of and is funded by a BBSRC CASE Studentship (BB/L016516/1), in partnership with Bayer Crop Sciences. Thanks go to Elisa Liras, Michael Schlemmer and Wolfgang Thielert of Bayer Crop Sciences for their support with this work. An equipment grant was also awarded by NERC Geophysical Equipment Facility for the use of the TLS during the pilot study. Martin J. Wooster is supported by the National Centre for Earth Observation (NCEO). A particular thanks goes to Nathan Wooster for assistance in collecting UAV data of the field for the bare ground DEM. The work at Rothamsted Research was supported by the Biotechnology and Biological Sciences Research Council (BBSRC) via the 20:20 Wheat®project (BBS/E/C/00005202) and the Enhancing Diversity in UK wheat through a public sector pre-breeding programme, the Wheat Improvement Strategic Programme (BB/I002278/1), and by the Department for Environment, Food and Rural Affairs (Defra) funded Wheat Genetic Improvement Network (IF0146).

Author Contributions: F.H.H., M.J.W., M.J.H. and A.B.R. conceived and designed the survey procedures. F.H.H., A.B.R. and M.C. performed the surveys. F.H.H., M.C. and A.M. processed and analysed the data. M.J.H., M.J.W. and A.B.R. provided feedback. F.H.H. wrote the paper.

Conflicts of Interest: The authors declare no conflict of interest. The founding sponsors had no role in the design of the study; in the collection, analyses, or interpretation of data; in the writing of the manuscript, and in the decision to publish the results.

References

1. Nelleman, C.; MacDavette, M.; Manders, T.; Eickhout, B.; Svihus, B.; Prins, A.G.; Kaltenborn, B.P. *The Environmental Food Crisis: The Environment's Role in Averting Future Food Crises*; A UNEP Rapid Response Assessment; UNEP/RID-Arendal: Arendal, Norway, 2009.
2. United Nations. *World Population Prospects: The 2015 Revision, Key Findings and Advance Tables*; United Nations: New York, NY, USA, 2015.
3. IDRC—International Development Research Centre. FACTS & FIGURES on Food and Biodiversity. Available online: https://www.idrc.ca/en/article/facts-figures-food-and-biodiversity (accessed on 22 May 2016).
4. Rothamsted Research. 20:20 Wheat. Available online: http://www.rothamsted.ac.uk/our-science/2020-wheat (accessed on 18 May 2016).

5. Cobb, J.N.; DeClerck, G.; Greenberg, A.; Clark, R.; McCouch, S. Next-generation phenotyping: Requirements and strategies for enhancing our understanding of genotype–phenotype relationships and its relevance to crop improvement. *Theor. Appl. Genet.* **2013**, *126*, 867–887. [CrossRef] [PubMed]
6. Gago, J.; Douthe, C.; Coopman, R.E.; Gallego, P.P.; Ribas-Carbo, M.; Flexas, J.; Escalona, J.; Medrano, H. UAVs challenge to assess water stress for sustainable agriculture. *Agric. Water Manag.* **2015**, *153*, 9–19. [CrossRef]
7. Saint Pierre, C.; Crossa, J.L.; Bonnett, D.; Yamaguchi-Shinozaki, K.; Reynolds, M.P. Phenotyping transgenic wheat for drought resistance. *J. Exp. Bot.* **2012**, *63*, 1799–1808. [CrossRef] [PubMed]
8. Araus, J.L.; Cairns, J.E. Field high-throughput phenotyping: The new crop breeding frontier. *Trends Plant Sci.* **2014**, *19*, 52–61. [CrossRef] [PubMed]
9. Chapman, S.C.; Merz, T.; Chan, A.; Jackway, P.; Hrabar, S.; Dreccer, M.F.; Holland, E.; Zheng, B.; Ling, T.J.; Jimenez-Berni, J. Pheno-Copter: A Low-Altitude, Autonomous Remote-Sensing Robotic Helicopter for High-Throughput Field-Based Phenotyping. *Agronomy* **2014**, *4*, 279–301. [CrossRef]
10. Torres, A.; Pietragalla, J. Chapter 19: Crop morphological traits. In *Physiological Breeding II: A Field Guide to Wheat Phenotyping*; Pask, A.J.D., Pietragalla, J., Mullan, D.M., Reynolds, M.P., Eds.; CIMMYT: Mexico D.F., Mexico, 2012; pp. 106–112.
11. Lati, R.N.; Filin, S.; Eizenberg, H. Estimating plant growth parameters using an energy minimization-based stereovision model. *Comput. Electron. Agric.* **2013**, *98*, 260–271. [CrossRef]
12. Zadoks, J.C.; Chang, T.T.; Konzak, C.F. A decimal code for the growth stages of cereals. *Weed Res.* **1974**, *14*, 415–421. [CrossRef]
13. Tottman, D.R. The decimal code for the growth stages of cereals, with illustrations. *Ann. Appl. Biol.* **1987**, *110*, 441–454. [CrossRef]
14. Agriculture and Horticulture Development Board. *Wheat Growth Guide*; AHDB: Warwickshire, UK, 2015.
15. Cornelissen, J.H.C.; Lavorel, S.; Garnier, E.; Díaz, S.; Buchmann, N.; Gurvich, D.E.; Reich, P.B.; Steege, H.T.; Morgan, H.D.; van der Heijden, M.G.A.; et al. A handbook of protocols for standardised and easy measurement of plant functional traits worldwide. *Aust. J. Bot.* **2003**, *51*, 335–380. [CrossRef]
16. Pérez-Harguindeguy, N.; Díaz, S.; Garnier, E.; Lavorel, S.; Poorter, H.; Jaureguiberry, P.; Bret-Harte, M.S.; Cornwell, W.K.; Craine, J.M.; Gurvich, D.E.; et al. New handbook for standardised measurement of plant functional traits worldwide. *Aust. J. Bot.* **2013**, *61*, 167–234. [CrossRef]
17. Tilly, N.; Hoffmeister, D.; Cao, Q.; Huang, S.; Lenz-Wiedemann, V.; Miao, Y.; Bareth, G. Multitemporal crop surface models: Accurate plant height measurement and biomass estimation with terrestrial laser scanning in paddy rice. *J. Appl. Remote Sens.* **2014**, *8*, 083671. [CrossRef]
18. Turner, D.; Lucieer, A.; de Jong, S.M. Time series analysis of landslide dynamics using an Unmanned Aerial Vehicle (UAV). *Remote Sens.* **2015**, *7*, 1736–1757. [CrossRef]
19. Woodget, A.S.; Carbonneau, P.E.; Visser, F.; Maddock, I.P. Quantifying submerged fluvial topography using hyperspatial resolution UAS imagery and structure from motion photogrammetry. *Earth Surf. Process. Landf.* **2015**, *40*, 47–64. [CrossRef]
20. Rango, A.; Laliberte, A.; Steele, C.; Herrick, J.E.; Bestelmeyer, B.; Schmugge, T.; Roanhorse, A.; Jenkins, V. Using unmanned aerial vehicles for rangelands: Current applications and future potentials. *Environ. Pract.* **2006**, *8*, 159–168. [CrossRef]
21. Laliberte, A.S.; Rango, A. Texture and scale in object-based analysis of subdecimeter resolution Unmanned Aerial Vehicle (UAV) imagery. *IEEE Trans. Geosci. Remote Sens.* **2009**, *47*, 761–770. [CrossRef]
22. Koh, L.; Wich, S. Dawn of drone ecology: Low-cost autonomous aerial vehicles for conservation. *Trop. Conserv. Sci.* **2012**, *5*, 121–132. [CrossRef]
23. Fernández-Hernandez, J.; González-Aguilera, D.; Rodríguez-Gonzálvez, P.; Mancera-Taboada, J. Image-based modelling from Unmanned Aerial Vehicle (UAV) photogrammetry: An effective, low-cost tool for archaeological applications. *Archaeometry* **2015**, *57*, 128–145. [CrossRef]
24. Berni, J.A.J.; Zarco-Tejada, P.J.; Gonzalez-Dugo, V.; Fereres, E. Remote sensing of thermal water stress indicators in peach. *Acta Hortic.* **2012**, *962*, 325–331. [CrossRef]
25. Panda, S.S.; Ames, D.P.; Panigrahi, S. Application of vegetation indices for agricultural crop yield prediction using neural network techniques. *Remote Sens.* **2010**, *2*, 673–696. [CrossRef]
26. Zarco-Tejada, P.J.; Suarez, L.; Gonzalez-Dugo, V. Spatial resolution effects on chlorophyll fluorescence retrieval in a heterogeneous canopy using hyperspectral imagery and radiative transfer simulation. *IEEE Geosci. Remote Sens. Lett.* **2013**, *10*, 937–941. [CrossRef]

27. Westoby, M.J.; Brasington, J.; Glasser, N.F.; Hambrey, M.J.; Reynolds, J.M. "Structure-from-Motion" photogrammetry: A low-cost, effective tool for geoscience applications. *Geomorphology* **2012**, *179*, 300–314. [CrossRef]
28. Konecny, G. Geoinformation: Remote Sensing, Photogrammetry and Geographic Information Systems, Second Edition. Available online: https://www.crcpress.com/Geoinformation-Remote-Sensing-Photogrammetry-and-Geographic-Information/Konecny/p/book/9781420068566 (accessed on 18 May 2016).
29. James, M.R.; Robson, S. Mitigating systematic error in topographic models derived from UAV and ground-based image networks: Mitigating systematic error in topographic models. *Earth Surf. Process. Landf.* **2014**, *39*, 1413–1420. [CrossRef]
30. Nex, F.; Remondino, F. UAV for 3D mapping applications: A review. *Appl. Geomat.* **2014**, *6*, 1–15. [CrossRef]
31. Bendig, J.; Willkomm, M.; Tilly, N.; Gnyp, M.L.; Bennertz, S.; Qiang, C.; Miao, Y.; Lenz-Wiedemann, V.I.S.; Bareth, G. Very high resolution crop surface models (CSMs) from UAV-based stereo images for rice growth monitoring in Northeast China. *Int. Arch. Photogramm. Remote Sens. Spat. Inf. Sci.* **2013**, *40*, 45–50. [CrossRef]
32. Bendig, J.; Bolten, A.; Bareth, G. UAV-based Imaging for Multi-Temporal, very high Resolution Crop Surface Models to monitor Crop Growth Variability. *Photogramm. Fernerkund. Geoinf.* **2013**, *2013*, 551–562. [CrossRef]
33. Ruiz, J.J.; Diaz-Mas, L.; Perez, F.; Viguria, A. Evaluating the accuracy of DEM generation algorithms from UAV imagery. *Int. Arch. Photogramm. Remote Sens. Spat. Inf. Sci.* **2013**, *40*, 333–337. [CrossRef]
34. Turner, D.; Lucieer, A.; Watson, C. An automated technique for generating georectified mosaics from Ultra-high resolution Unmanned Aerial Vehicle (UAV) imagery, based on Structure from Motion (SfM) point clouds. *Remote Sens.* **2012**, *4*, 1392–1410. [CrossRef]
35. Aasen, H.; Burkart, A.; Bolten, A.; Bareth, G. Generating 3D hyperspectral information with lightweight UAV snapshot cameras for vegetation monitoring: From camera calibration to quality assurance. *ISPRS J. Photogramm. Remote Sens.* **2015**, *108*, 245–259. [CrossRef]
36. Geipel, J.; Link, J.; Claupein, W. Combined spectral and spatial modeling of corn yield based on aerial images and crop surface models acquired with an unmanned aircraft system. *Remote Sens.* **2014**, *6*, 10335–10355. [CrossRef]
37. Willkomm, M.; Bolten, A.; Bareth, G. Non-destructive monitoring of rice by hyperspectral in-field spectrometry and UAV-based remote sensing: Case study of field-grown rice in north Rhine-Westphalia, Germany. *ISPRS Int. Arch. Photogramm. Remote Sens. Spat. Inf. Sci.* **2016**, *XLI-B1*, 1071–1077. [CrossRef]
38. Barraclough, P.B.; Howarth, J.R.; Jones, J.; Lopez-Bellido, R.; Parmar, S.; Shepherd, C.E.; Hawkesford, M.J. Nitrogen efficiency of wheat: Genotypic and environmental variation and prospects for improvement. *Eur. J. Agron.* **2010**, *33*, 1–11. [CrossRef]
39. Haala, N.; Rothermel, M. Dense multiple stereo matching of highly overlapping UAV imagery. *ISPRS Int. Arch. Photogramm. Remote Sens. Spat. Inf. Sci.* **2012**, *39*, B1. [CrossRef]
40. Hartmann, W.; Tilch, S.; Eisenbeiss, H.; Schindler, K. Determination of the UAV position by automatic processing of thermal images. *ISPRS Int. Arch. Photogramm. Remote Sens. Spat. Inf. Sci.* **2012**, *39*, B6. [CrossRef]
41. Agisoft. *Agisoft PhotoScan User Manual Professional Edition*, version 1.2; AgiSoft LLC, 2016. Available online: http://www.agisoft.com/downloads/user-manuals/ (accessed on 2 February 2016).
42. Granshaw, S.I. Photogrammetric terminology: Third edition. *Photogramm. Rec.* **2016**, *31*, 210–252. [CrossRef]
43. Leica Geosystems. Leica Cyclone 3D Point Cloud Processing Software. Available online: http://leica-geosystems.com/products/laser-scanners/software/leica-cyclone (accessed on 16 April 2016).
44. Pask, A.J.D.; Pietragalla, J.; Mullan, D.M.; Reynolds, M.P. *Physiological Breeding II: A Field Guide to Wheat Phenotyping*; CIMMYT: Mexico, Mexico, 2012.
45. Bareth, G.; Bendig, J.; Tilly, N.; Hoffmeister, D.; Aasen, H.; Bolten, A. A comparison of UAV- and TLS-derived plant height for crop monitoring: Using polygon grids for the analysis of Crop Surface Models (CSMs). *Photogramm. Fernerkund. Geoinf.* **2016**, *2016*, 85–94. [CrossRef]
46. Jay, S.; Rabatel, G.; Hadoux, X.; Moura, D.; Gorretta, N. In-field crop row phenotyping from 3D modeling performed using Structure from Motion. *Comput. Electron. Agric.* **2015**, *110*, 70–77. [CrossRef]
47. Virlet, N.; Sabermanesh, K.; Sadeghi-Tehran, P.; Hawkesford, M.J. Field Scanalyzer: An automated robotic field phenotyping platform for detailed crop monitoring. *Funct. Plant Biol.* **2016**, *44*, 143–153. [CrossRef]

48. Andrade-Sanchez, P.; Gore, M.A.; Heun, J.T.; Thorp, K.R.; Carmo-Silva, A.E.; French, A.N.; Salvucci, M.E.; White, J.W. Development and evaluation of a field-based high-throughput phenotyping platform. *Funct. Plant Biol.* **2014**, *41*, 68–79. [CrossRef]
49. Comar, A.; Burger, P.; de Solan, B.; Baret, F.; Daumard, F.; Hanocq, J.-F. A semi-automatic system for high throughput phenotyping wheat cultivars in-field conditions: Description and first results. *Funct. Plant Biol.* **2012**, *39*, 914–924. [CrossRef]
50. Honkavaara, E.; Saari, H.; Kaivosoja, J.; Pölönen, I.; Hakala, T.; Litkey, P.; Mäkynen, J.; Pesonen, L. Processing and assessment of spectrometric, stereoscopic imagery collected using a lightweight UAV spectral camera for precision agriculture. *Remote Sens.* **2013**, *5*, 5006–5039. [CrossRef]
51. Sankaran, S.; Khot, L.R.; Espinoza, C.Z.; Jarolmasjed, S.; Sathuvalli, V.R.; Vandemark, G.J.; Miklas, P.N.; Carter, A.H.; Pumphrey, M.O.; Knowles, N.R.; et al. Low-altitude, high-resolution aerial imaging systems for row and field crop phenotyping: A review. *Eur. J. Agron.* **2015**, *70*, 112–123. [CrossRef]
52. Bendig, J.; Yu, K.; Aasen, H.; Bolten, A.; Bennertz, S.; Broscheit, J.; Gnyp, M.L.; Bareth, G. Combining UAV-based plant height from crop surface models, visible, and near infrared vegetation indices for biomass monitoring in barley. *Int. J. Appl. Earth Obs. Geoinf.* **2015**, *39*, 79–87. [CrossRef]
53. Berni, J.; Zarco-Tejada, P.J.; Suarez, L.; Fereres, E. Thermal and narrowband multispectral remote sensing for vegetation monitoring from an unmanned aerial vehicle. *IEEE Trans. Geosci. Remote Sens.* **2009**, *47*, 722–738. [CrossRef]
54. Prashar, A.; Jones, H.G. Infra-red thermography as a high-throughput tool for field phenotyping. *Agronomy* **2014**, *4*, 397–417. [CrossRef]